www.sciencemag.org/cgi/content/full/science.1182369/DC1

# Supporting Online Material for

## A Stratified Redox Model for the Ediacaran Ocean

Chao Li,* Gordon D. Love, Timothy W. Lyons, David A. Fike, Alex L. Sessions, Xuelei Chu

*To whom correspondence should be addressed. E-mail: chaoli@ucr.edu

Published 11 February 2010 on *Science* Express
DOI: 10.1126/science.1182369

**This PDF file includes:**

# Supporting Online Material (SOM)

## A Stratified Redox Model for the Ediacaran Ocean

Chao Li, Gordon D. Love, Timothy W. Lyons, David A. Fike,
Alex L. Sessions, Xuelei Chu

### Materials and methods

#### *Sample preparation*

All outcrop samples were collected on a field trip to South China in March 2007. Large blocks (>200 g) of the freshest exposures were deliberately targeted for sampling. The large rock blocks were subsequently trimmed by a water-cooled rock saw or by hammer in the laboratory to remove the potentially weathered surfaces and then broken into small pieces. The pieces were further crushed into powders using a SPEX 8515 Shatterbox with an alumina (ceramic) puck. Rock pieces that contained readily visible pyrite nodules or bands were discarded prior to crushing.

#### *Total organic carbon (TOC) and total inorganic carbon (TIC)*

TOC was determined as the difference between total carbon (TC) and total inorganic carbon (TIC) measured using a CS-500 carbon/sulfur analyzer with a high-temperature furnace and acidification module (Eltra, Germany). For TC, ~100 mg of sample powder were weighed into a ceramic boat and combusted in pure (99.95%) $O_2$ at 1350 °C for ~3 min. The total carbon liberated was then measured by infrared spectral absorption of the evolved $CO_2$. For TIC, ~100 mg of sample powder were reacted with 20% HCl, heated at 50 °C and stirred. TIC was also quantified by infrared absorption detection of the $CO_2$ generated. Analytical errors for TOC and TIC are ±0.1 wt% based on analysis of carbonate standard AR1034 (Alpha, USA).

#### *Pyrite sulfur isotopes ($\delta^{34}S_{py}$) and concentrations*

Disseminated pyrite concentrations and isotopic compositions were analyzed by the chromium reduction method (*S1*). Pyrite extraction was performed under $N_2$ by the addition of 20 ml of concentrated HCl and 40 ml of 1M chromous chloride solution. The reaction mixture was heated for 2 h, with the liberated sulfide collected either as silver sulfide after bubbling through 30 ml of 3 wt% silver nitrate solution with 10% $NH_4OH$ by volume (for isotopic analysis) or as zinc sulfide after bubbling through 30 ml of 3 wt% zinc acetate with 10% $NH_4OH$ by volume for pyrite-S concentration. Mean recovery of parallel replicate pure pyrite standards was 105.6%. Filtered, rinsed and dried $Ag_2S$ precipitates were combined with an excess of $V_2O_5$ and analyzed for S-isotope composition following online combustion using a Thermo Instruments Delta V Plus isotope ratio mass spectrometer coupled with a Costech elemental analyzer at the University of California, Riverside. Sulfur isotope compositions are expressed as $\delta^{34}S = (R_{sample}/R_{standard} - 1) \times 1000$, where R is the ratio of $^{34}S/^{32}S$, reported as permil (‰)

deviations from V-CDT international standard. The analytical error was ~0.1‰ (1σ), calculated from replicate analyses of IAEA international standards. Samples were calibrated using the same international standards: IAEA S1 (-0.3‰), IAEA S2 (22.65‰) and IAEA S3 (-32.5‰). To determine concentrations of pyrite S, the ZnS precipitates were acidified with 10 ml of 6 M HCl to re-liberate the sulfur, followed by titration with a 0.1 M $KIO_3$ solution in the presence of excess KI and starch.

### *Carbonate-associated sulfate (CAS) concentrations and isotopes ($\delta^{34}S_{CAS}$)*

Carbonate samples (with carbonate contents typical >30 wt% of the total rock) were powdered, leached of soluble sulfates in a 10% NaCl solution, followed by three rinses in DI water and dissolved in 3N HCl. The acidified samples were filtered, and an excess of 1M $BaCl_2$ was added to the filtrate to precipitate $BaSO_4$. The $BaSO_4$ precipitate was rinsed, filtered, dried and then combined with an excess of $V_2O_5$ and analyzed for its S-isotope composition at the University of California, Riverside, following online combustion. Sulfur isotope compositions are expressed in standard δ-notation as permil (‰) deviations from V-CDT, with an analytical error of ~0.1‰ calculated from replicate analyses of samples and laboratory standards: NBS 127 (21.1‰), IAEA SO-5 (0.49‰) and IAEA SO-6 (-34.05‰). CAS concentrations were calculated based on the mass of $BaSO_4$ precipitate and are listed as a proportion of total rock mass (ppm of rock) in Table S1.

### *Elemental analyses*

For elemental analysis of Mo, Al and total Fe, we used a standard multi-acid digestion ($HNO_3$–HCl–HF). We specifically used distilled $HNO_3$ and HCl and trace-metal grade HF reagents for all our samples. An aliquot of powdered sample was weighed into a porcelain crucible, ashed at 850$^o$C for 12 h and weighed again after cooling. The mass lost on ignition (LOI) was recorded and used later for correction of the elemental abundances. About 100 mg of ashed sample were weighed accurately in a 15 ml Savillex Teflon bomb equipped with a screw cap. The sample was first digested by adding ~0.2 ml water and ~1 ml concentrated $HNO_3$ and heated at 200$^o$C for 2 h. The sample was then transferred to a sterile 15 ml centrifuge tube after cooling and spun at 6,000 r.p.m. for 5 min. The supernatant was removed and retained, while the residual undigested sample was returned to the Teflon bomb. The purpose of this step was to remove cations such as $Ca^{2+}$ (primarily from carbonates) that can form insoluble fluoride precipitates during reaction with HF. For carbonate-rich samples, this step was repeated. The sample residue was further digested by adding ~0.2 ml water and ~ 1 ml $HNO_3$/HF (1:2) and heated at 200$^o$C for at least 24 h. The sample was subsequently dried down in order to evaporate the acids. The last digestion was in ~ 0.2 ml water and ~1 ml concentrated HCl, which was heated at 200$^o$C for at least 2 h. If the rock powders were not completely digested after this treatment, additional rounds of digestion were performed. After complete digestion, we returned the $HNO_3$ supernatant to the Teflon bomb. Following an evaporation step to remove concentrated acid, we diluted the sample 2,000-fold in 2% nitric acid and analyzed it for the target elements on a quadrupole inductively coupled plasma mass spectrometer (ICP-MS). The replicate digestions of USGS standards (SDO; n = 7) produce analytical errors of 1.1 %, 1.4 % and 10.4 % for

assays of Al, Fe and Mo, respectively, although the typical analytical error from ICP-MS runs alone was less than 1%.

***Iron speciation analyses***

The iron content associated with pyrite ($Fe_{py}$) in rock samples was calculated stoichiometrically based on the pyrite sulfur concentrations obtained from chromium reduction described above (Section 1.3). $Fe_{carb}$, $Fe_{ox}$ and $Fe_{mag}$ were measured by a sequential extraction procedure described previously (*S2*). The reaction volume was 10 ml for all sequential extractions described below. In addition, a centrifugation step to remove the supernatant was performed between extractions. Step 1 (sodium acetate extraction for $Fe_{carb}$): about 100 mg rock powders were weighed accurately in a 15 ml sterile centrifuge tube and extracted in a 50$^{o}$C water bath for 48 h with shaking using 1M sodium acetate solution adjusted to pH = 4.5 by addition of trace-metal grade acetic acid. Step 2 (sodium dithionite extraction for $Fe_{ox}$): the sample residue from step 1 was further extracted using a 50 g/l sodium dithionite solution buffered to pH = 4.8 with 0.2 M sodium citrate and trace-metal grade acetic acid in a 50$^{o}$C water bath for 2 h with shaking. Step 3 (ammonium oxalate extraction for $Fe_{mag}$): the sample residue from step 2 was then extracted by a 0.2 M ammonium oxalate/0.17 M oxalic acid solution in 50$^{o}$C water bath for 6 h with shaking. All extracts were diluted 100 fold in 2% nitric acid and analyzed for their Fe contents on a quadrupole ICP-MS (see section 1.5).

***Carbon isotopic compositions of carbonates ($\delta^{13}C_{carb}$) and TOC ($\delta^{13}C_{org}$)***

Carbonate-C isotopic compositions were measured at the University of California, Riverside (UCR) and at the University of Missouri (MU) and are reported using the standard $\delta^{13}C$ notation compared to VPDB. At UCR, carbonate $CO_2$ was extracted in a Gas Bench II with 100% phosphoric acid for 1 hour at 70ºC and analyzed using a Thermo Instruments Delta V plus Mass Spectrometer. Delta values were calibrated relative to international reference standards LSVEC and NBS-19, and the external error for standards run with samples was 0.01‰ for carbon. At MU, carbonate $CO_2$ was extracted on a Kiel Carb III device connected to a Thermo Finnigan Delta$^{+}$ Mass Spectrometer. External error for an international standard (NBS-19) run with the samples was 0.02‰ for carbon. Isotopic compositions of TOC were measured at Caltech. Rock powders were first decarbonated with 4M HCl at room temperature for >12 hours. Some samples were further treated with HF to remove large amount of silicates. The organic residue was then washed with deionized water and homogenized after drying in a 50°C oven. Values for $\delta^{13}C_{org}$ were measured on a Costech elemental analyzer (ECS4010) coupled to a Finnigan MAT Delta S isotope ratio mass spectrometer. Samples were calibrated against two standards, Indiana University Urea (-34.22 ± 0.02‰) and Indiana University Acetanilide (-29.52 ± 0.02‰). The standard deviation for measurements of all standards was <0.2‰ (n = 94).

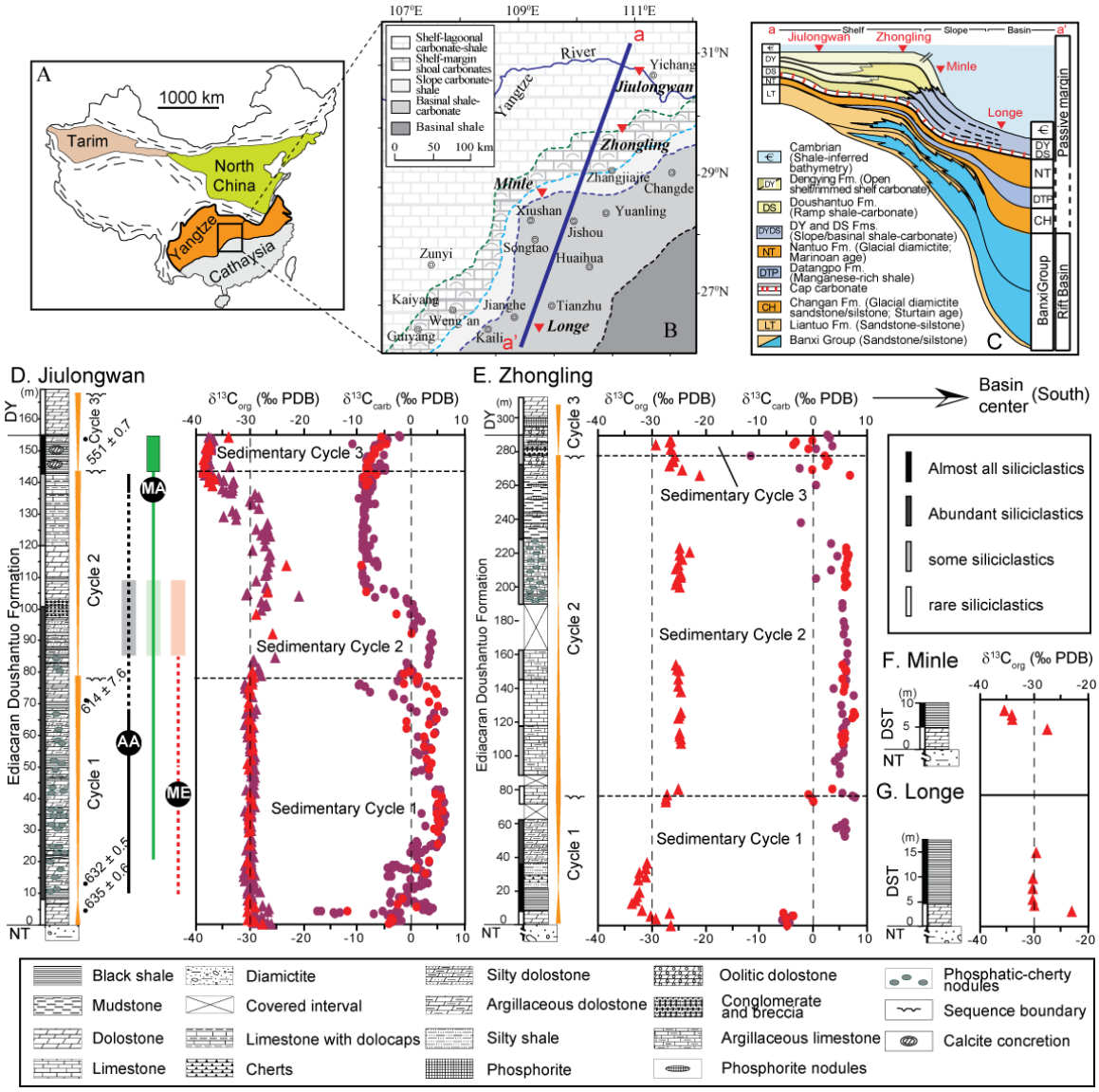


**Figure S1.** Geological background for the Doushantuo Formation. (A) The tectonic location of the studied area in South China (adapted after *S3*). (B) Paleogeographic reconstruction of the Yangtze platform (i.e., Nanhua Basin) during deposition of the middle and upper Doushantuo Formation and the locations of the four sections sampled for this study (as indicated by triangles) (after *S4*). (C) A conceptual transect from north to south showing the general stratigraphy in the Nanhua Basin and the relative palaeodepths of the four sections (after *S5*). (D-G) Litho-, sequence- and C-isotope-stratigraphies of the studied sections. Sequence stratigraphic data and C-isotope data in red are from *S3* for the Jiulongwan section and from *S6* for the Zhongling section. The C-isotope data in purple are from this study. For the inner shelf Jiulongwan section, available geochronological and paleontological data obtained from Yangtze Gorges area and Weng'an (Guizhou province) are also included. Age data are from *S7* and *S8*. Key paleontological data for Doushantuo Formation are simplified from *S3*. AA: Acanthomorphic acritarchs; MA: multicelllular algae; ME: Metazoan embryos. The shaded bars show fossil stratigraphic ranges based on first and last occurrences from the Weng'an section in Guizhou province. Most

available geochronological and paleontological data are from the shelf sections. Samples were collected only from the horizons where fresh/unweathered rocks were available. Formations: DY-Dengying; NT-Nantuo; DST-Doushantuo.

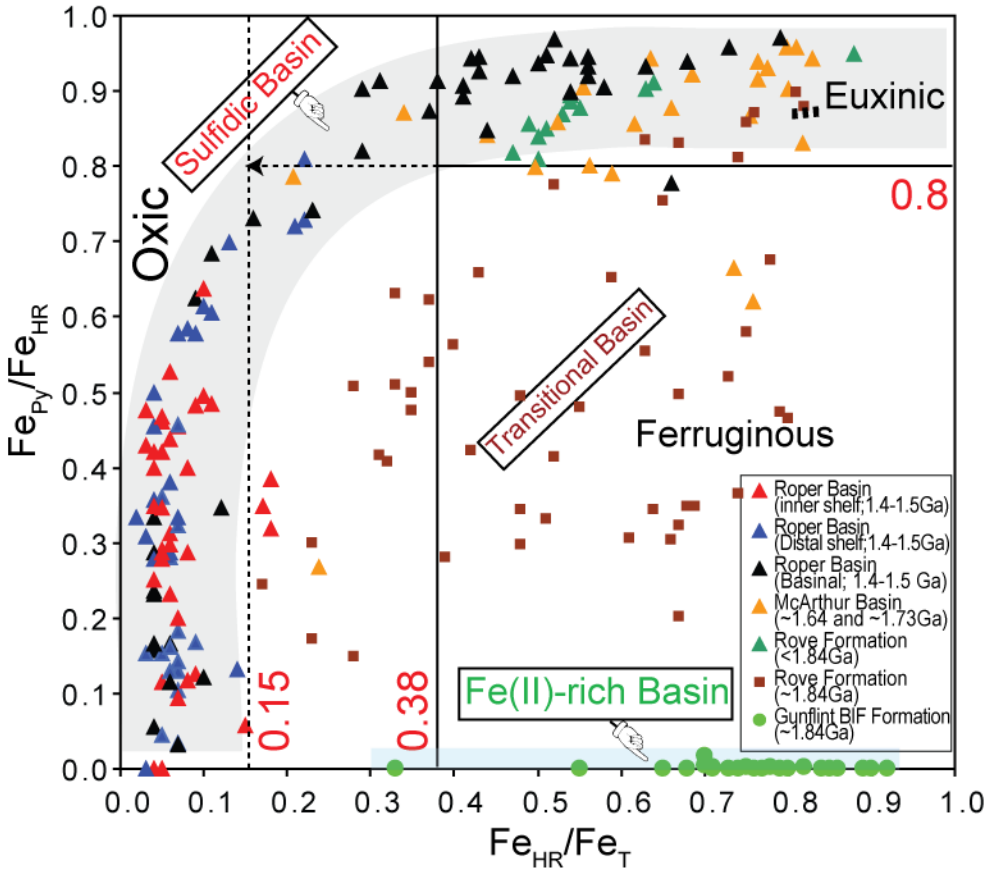


**Figure S2.** $Fe_{Py}/Fe_{HR}$ versus $Fe_{HR}/Fe_T$ data for samples from Paleo- and Mesoproterozoic basins, with end-member redox conditions denoted on the crossplot. Data are from references *S9*, *S10* and *S11*. For the Fe(II)-rich basin, represented here by data from Gunflint Banded Iron Formation (Canada), sedimentary rocks deposited below the chemocline yielded $Fe_{HR}/Fe_T$ ratios >0.15 (the cutoff for anoxia for highly mature ancient rocks (*S12*), as assumed for our Doushantuo rock dataset), and most of them were >0.38 [the cutoff for immature rocks and modern sediments (*S12*)], but with extremely low values for $Fe_{Py}/Fe_{HR}$ (typically below 0.05). In contrast, for euxinic basins with sulfidic deep waters represented here by data from the Roper Basin (Australia), the McArthur Basin (Australia) and the upper Rove Formation (Canada), $Fe_{Py}/Fe_{HR}$ ratios were high ($\geq$0.8), and $Fe_{HR}/Fe_T$ ratios were >0.15 for sedimentary rocks deposited below the chemocline, indicating anoxic and sulfidic conditions. Those samples deposited at shallow water depths beneath oxic surface waters ($Fe_{HR}/Fe_T$ <0.15) also yielded high $Fe_{Py}/Fe_{HR}$ ratios, suggesting abundant hydrogen sulfide confined to the pore waters. Samples collected from a basin interpreted as a transitional redox state represented here by lower Rove Formation (Canada) plot in intermediate zones between these two end-member profiles, consistent with anoxic bottom waters with elevated dissolved iron by minimal $H_2S$.

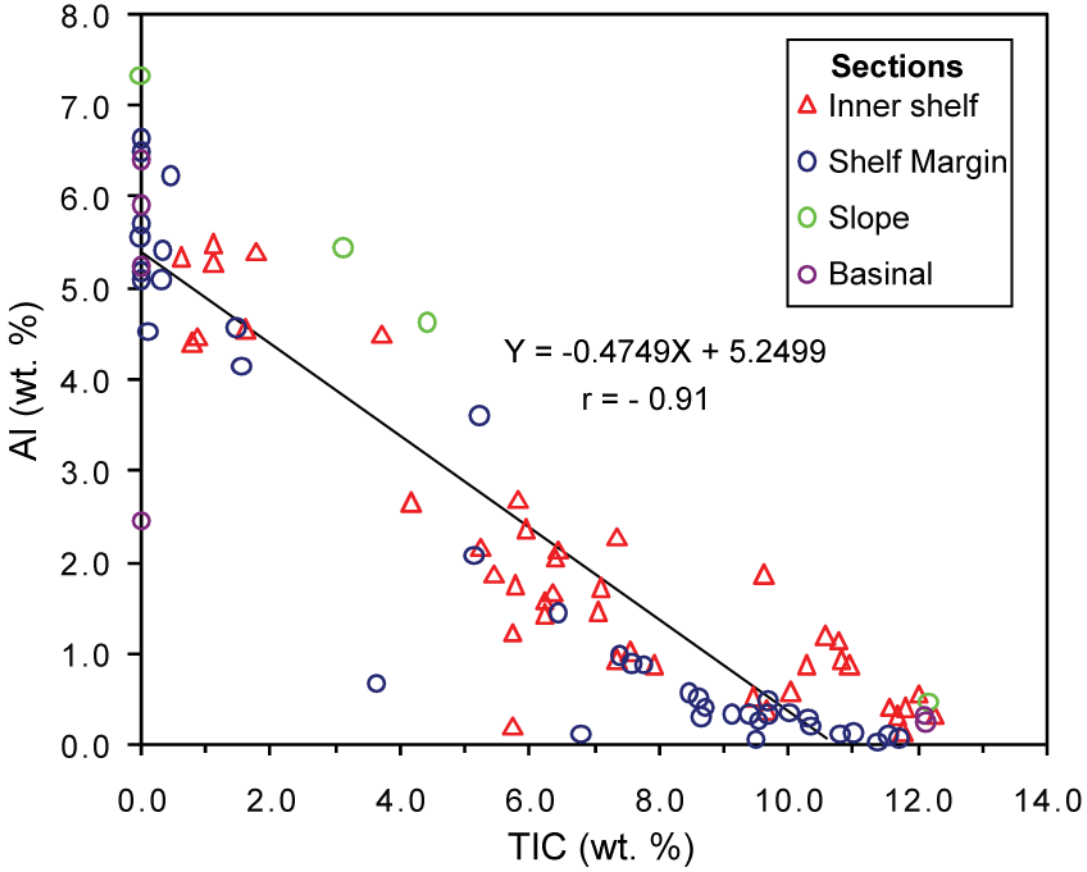


**Figure S3.** A strong negative correlation is seen between carbonate and detrital Al contents for sedimentary rocks from the Doushantuo Formation in this study. TIC is total inorganic (carbonate) carbon. Data are from the inner shelf (Jiulongwan), shelf margin (Zhongling), slope (Minle) and basin (Longe) sections.

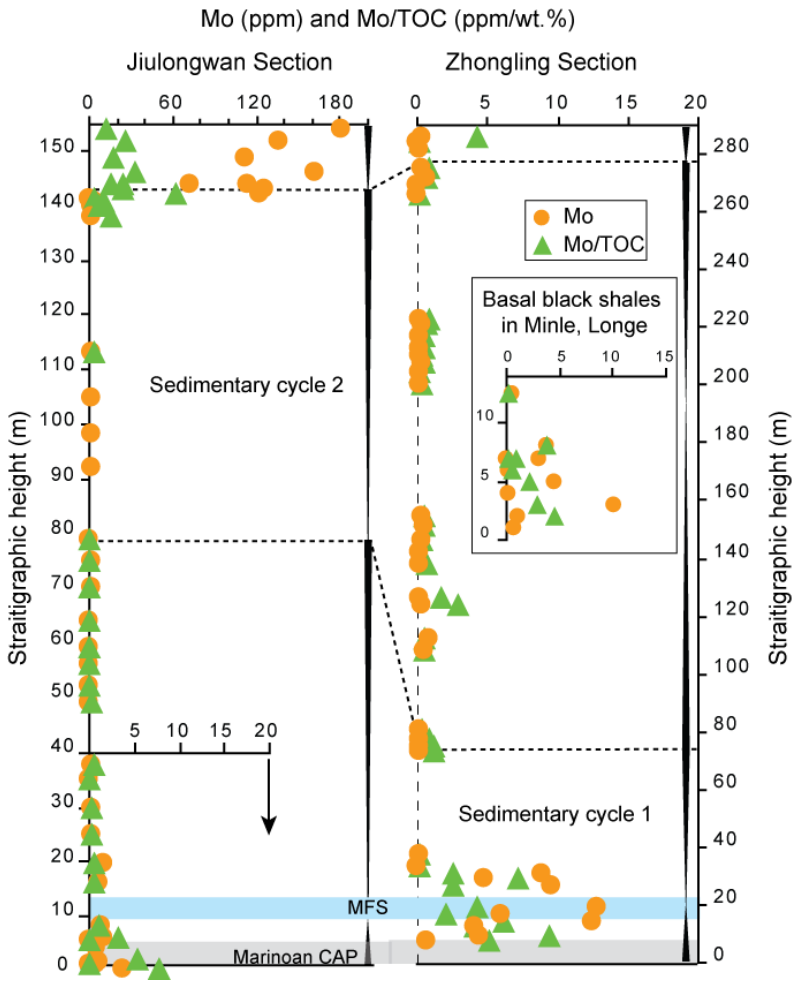


**Figure S4.** Stratigraphic comparisons of Mo and Mo/TOC for the Doushantuo Formation for sections from the inner shelf (left panel) and shelf margin (right panel). Stratigraphic correlation of the two sections is based on published sequence stratigraphic data (*S3*, *S6*) and three similar transgressive-regressive sedimentary cycles can be identified at both sections. The samples that plot at the euxinic end of Path A in Fig. 1B in the main text are generally from two stratigraphic levels: the uppermost late Ediacaran black shales from inner shelf Jiulongwan section and the early Ediacaran black shales from the shelf margin Zhongling section at and around the deglacial maximum flooding surface (MFS in blue band) (*S6*). Both these sample sets demonstrate local Mo enrichments (as also seen in elevated Mo/TOC) above typical crustal values of <2 ppm, as expected given their independently inferred deposition under euxinic waters. The magnitude of Mo and Mo/TOC enrichment in late Ediacaran rocks from the Jiulongwan section is significantly greater than for the lower Ediacaran rocks from the Zhongling section (Table S1), consistent with a stepwise and protracted oxidation of the ocean through Ediacaran time (*S13, S14*). Some evidence suggesting restricted marine circulation for the inner shelf setting of the lower Doushantuo Formation (Cycle 1) (*S15*) may be gleaned from the lack of any discernible Mo enrichment in rocks with high $Fe_{Py}/Fe_{HR}$ (see Fig S6) in contrast to appreciable Mo enrichment seen in apparently time-equivalent, more distal black shales from the Zhongling section. This lateral variation does not invalidate our proposed ocean redox structure or our hypothesis for lateral sulfate concentration and isotope gradients, because the detailed geochemical arguments behind these models are expressed over the entire 84 Ma of deposition of the Doushantuo Formation extending into the late Ediacaran (551 Ma).

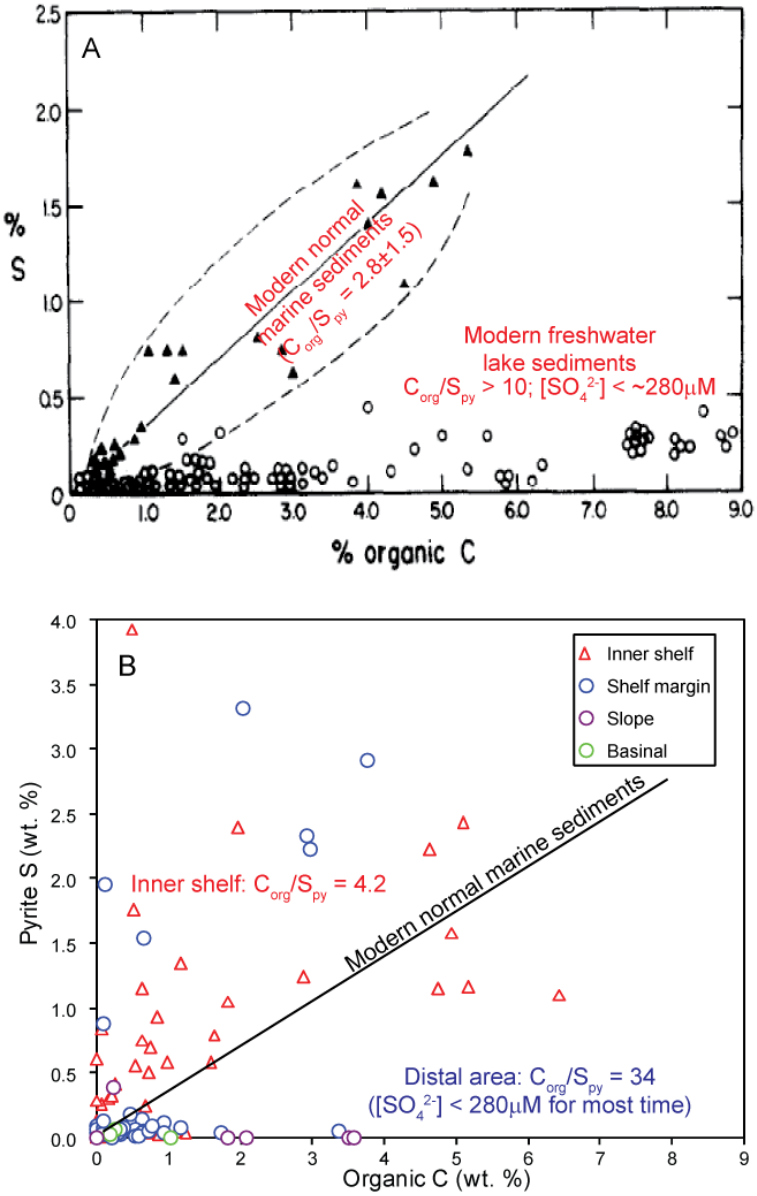


**Figure S5.** Pyrite S ($S_{py}$) versus organic C ($C_{org}$) contents for (A) modern normal marine and freshwater lake sediments (after reference *S16*) and (B) sedimentary rocks from the Doushantuo Formation. In organic-rich sediments deposited beneath freshwater aquatic systems, such as lakes and rivers, much higher $C_{org}/S_{py}$ ratios (>10) are observed compared to analogous marine sediments because of the much lower concentrations of dissolved sulfate relative to seawater (*S17, S18*). The average $C_{org}/S_{py}$ ratio of the inner shelf Jiulongwan section is 4 ($n$=42) but is much higher (34, $n$=49) in the distal sections. This relationship argues for a decrease in sulfate content from the shore to distal settings, reaching extremely low values. In addition, black shale samples from the deep basinal Longe section have organic C contents ranging from 1.8 – 3.6 wt.%, yet very little or no pyrite was found in these samples (Table S1). This relationship suggests that sulfate availability rather than organic matter limited the bacterial sulfate reduction required to initiate and sustain pyrite formation in the distal portions of the Nanhua Basin.

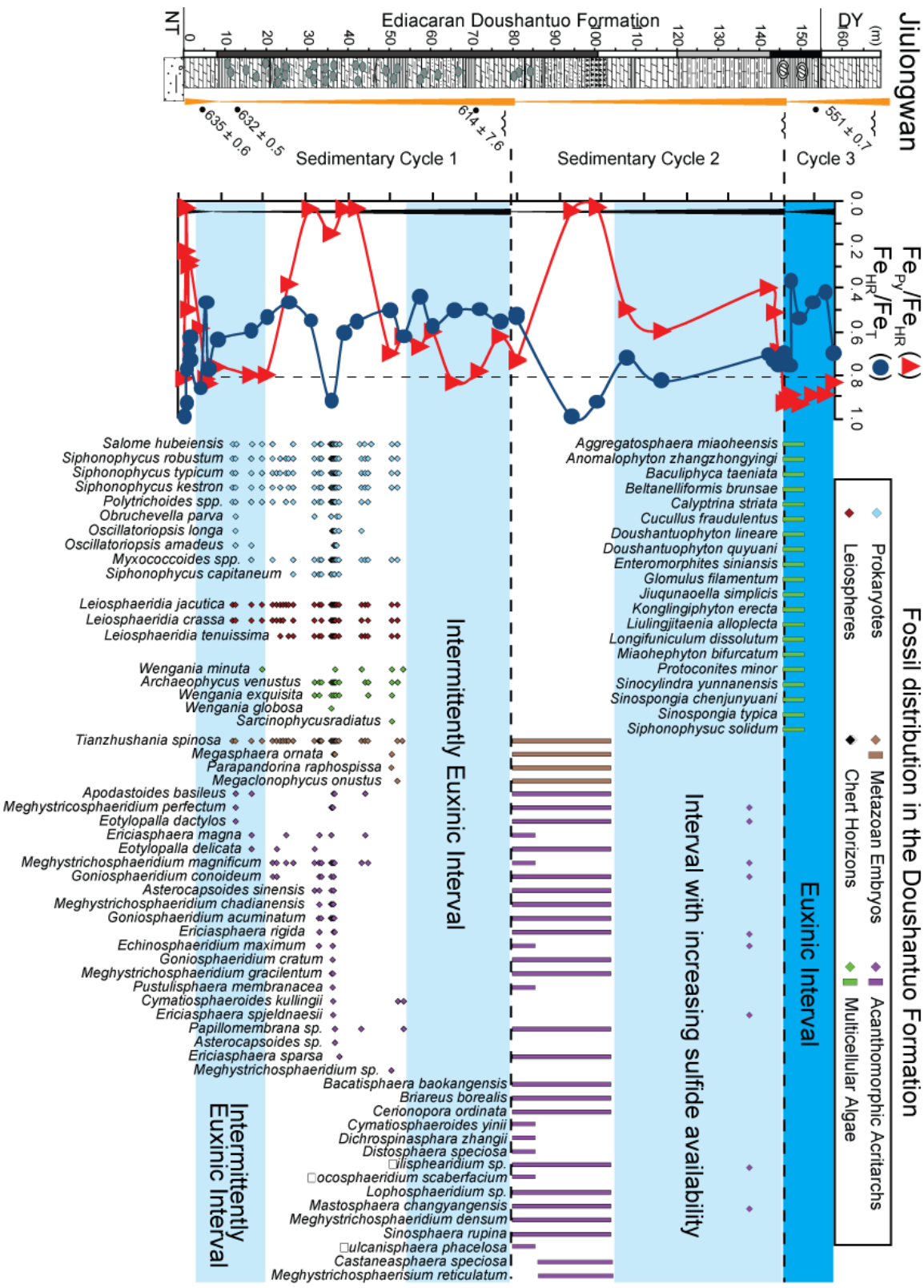
Jiulongwan
Ediacaran Doushantuo Formation
NT
DY
(m)
635 ± 0.6
632 ± 0.5
614 ± 7.6
551 ± 0.1
Sedimentary Cycle 1
Sedimentary Cycle 2
Cycle 3
Fe_Py/Fe_HR (▲)
Fe_HR/Fe_T (●)
Fossil distribution in the Doushantuo Formation
Prokaryotes
Metazoan Embryos
Acanthomorphic Acritarchs
Leiospheres
Chert Horizons
Multicellular Algae
Salome hubeiensis
Siphonophycus robustum
Siphonophycus typicum
Siphonophycus kestron
Polytrichoides spp.
Obruchevella parva
Oscillatoriopsis longa
Oscillatoriopsis amadeus
Myxococcoides spp.
Siphonophycus capitaneum
Leiosphaeridia jacutica
Leiosphaeridia crassa
Leiosphaeridia tenuissima
Wengania minuta
Archaeophycus venustus
Wengania exquisita
Wengania globosa
Sarcinophycusradiatus
Tianzhushania spinosa
Megasphaera ornata
Parapandorina raphospissa
Megaclonophycus onustus
Apodastoides basileus
Meghystricosphaeridium perfectum
Eotylopalla dactylos
Ericiasphaera magna
Eotylopalla delicata
Meghystrichosphaeridium magnificum
Goniosphaeridium conoideum
Asterocapsoides sinensis
Meghystrichosphaeridium chadianensis
Goniosphaeridium acuminatum
Ericiasphaera rigida
Echinosphaeridium maximum
Goniosphaeridium cratum
Meghystrichosphaeridium gracilentum
Pustulisphaera membranacea
Cymatiosphaeroides kullingii
Ericiasphaera spjeldnaesii
Papillomembrana sp.
Asterocapsoides sp.
Ericiasphaera sparsa
Meghystrichosphaeridium sp.
Bacatisphaera baokangensis
Briareus borealis
Cerionopora ordinata
Cymatiosphaeroides yinii
Dichrospinasphara zhangii
Distosphaera speciosa
□ilisphearidium sp.
□ocosphaeridium scaberfacium
Lophosphaeridium sp.
Mastosphaera changyangensis
Meghystrichosphaeridium densum
Sinosphaera rupina
□ulcanisphaera phacelosa
Castaneasphaera speciosa
Meghystrichosphaerisium reticulatum
Aggregatosphaera miaoheensis
Anomalophyton zhangzhongyingi
Baculiphyca taeniata
Beltanelliformis brunsae
Calyptrina striata
Cucullus fraudulentus
Doushantuophyton lineare
Doushantuophyton quyuani
Enteromorphites siniansis
Glomulus filamentum
Jiuqunaoella simplicis
Konglingiphyton erecta
Liulingjitaenia alloplecta
Longifuniculum dissolutum
Miaohephyton bifurcatum
Protoconites minor
Sinocylindra yunnanensis
Sinospongia chenjunyuani
Sinospongia typica
Siphonophysuc solidum
Intermittently Euxinic Interval
Euxinic Interval
Interval with increasing sulfide availability
Intermittently Euxinic Interval

**Figure S6.** Stratigraphic variations for $Fe_{py}/Fe_{HR}$, $Fe_{HR}/Fe_T$ and fossil occurrences for the inner shelf sedimentary facies of the Doushantuo Formation. The iron speciation data derive from this study, while the fossil and sequence stratigraphy data are from a compilation reported in reference *S3*. Note that the fossil occurrences in sedimentary Cycle 1 are from our Jiulongwan section; fossil occurrences in sedimentary Cycle 2 are from the nearby Tianjiayuanzi section (diamonds) in the Yangtze Gorges and the Weng'an section (bars) in Guizhou Province. The fossils in sedimentary Cycle 3 reflect occurrences from the nearby Miaohe section. Diamonds indicate actual stratigraphic occurrences; bars depict stratigraphic ranges based on first and last occurrences. It appears that the most diverse assemblages of Ediacaran acanthomorphic acritarchs and metazoan embryo fossils from the Doushantuo Formation in South China are associated with stratigraphic intervals deposited when toxic hydrogen sulfide was extremely low in the water column (i.e., intervals with the lowest $Fe_{py}/Fe_{HR}$ values, approaching zero) regardless of indications of anoxia (i.e., high $Fe_{HR}/Fe_T$ values). In contrast, multicellular algal fossils (presumably planktonic) could be detected in extremely euxinic intervals. These results strongly support our proposed redox model and its relationship to the patchy animal fossil record of the Ediacaran. The occurrences of metazoan fossils in non-sulfidic but anoxic (i.e., ferruginous) waters were likely related to i) the resting stages in early metazoan life cycles as an evolutionary/protective response to episodes of bottom water anoxia without the deleterious toxic effects of hydrogen sulfide in Ediacaran shelf/platform environments (*S19*), as well as to ii) the relatively shorter distances of lateral transport of sediment and metazoan bodies from the oxic shallow seafloor into ferruginous waters below the oxycline in comparison to delivery into euxinic waters farther along the shelf.

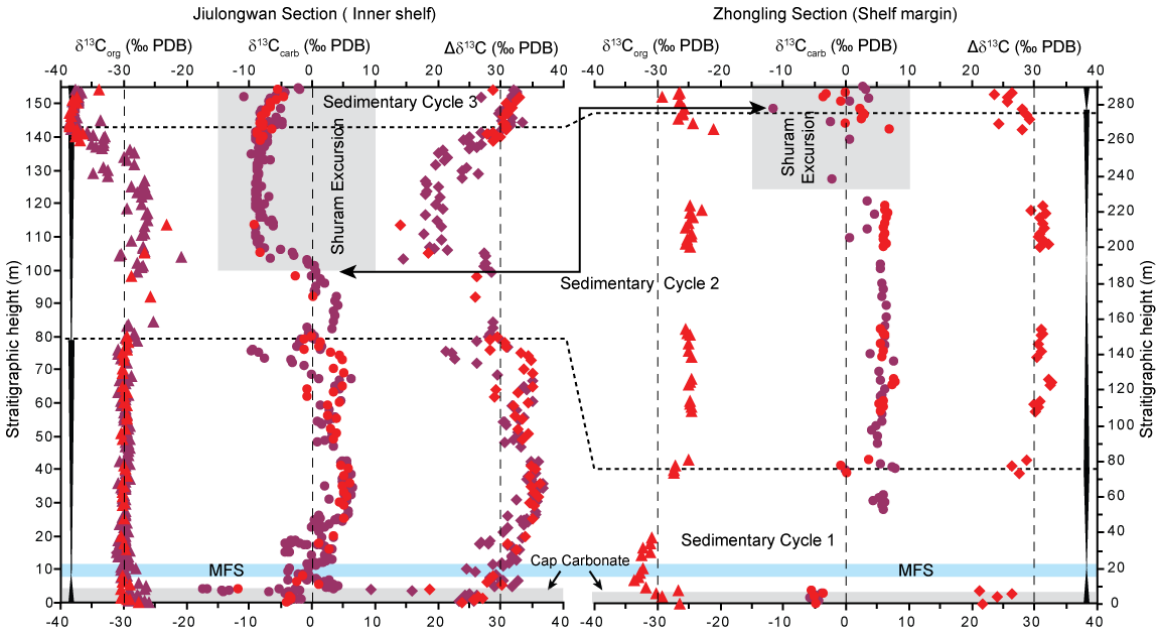


**Figure S7.** Carbon isotope chemostratigraphy of the Doushantuo Formation for the inner shelf section at Jiulongwan (left panel) and the shelf margin section at Zhongling (right panel). See Fig. S4 for an explanation of the sequence stratigraphic framework provided in this figure. C-isotope data in purple for the Jiulongwan and Zhongling sections are from references *S3* and *S6*, respectively, while the data in red are from this study. One of the most important features of Ediacaran chemostratigraphy is recognition of the Shuram C-isotope excursion characterized by a significant interval of $^{13}$C-depleted carbonates ($\delta^{13}C_{carb}$) with isotopic compositions below average mantle values (-5‰). As for the Ediacaran strata from the Huqf Supergroup of South Oman (*S14*), this anomaly occurs in association with a decoupling of C-isotope records for coeval carbonate and sedimentary organic matter ($\delta^{13}C_{org}$). The Shuram excursion is well expressed in the Jiulongwan section but less so in the Zhongling section, where only a few carbonate samples from the uppermost Doushantuo Formation possess $\delta^{13}$C values near -5‰. The gray areas delineated in the $\delta^{13}C_{carb}$ records from both sections indicate our best estimate of the Shuram excursion interval, and the double-headed arrow indicates inferred correlation points based on C-isotope chemostratigraphy. Using this method of correlation, a ~15‰ difference in $\delta^{34}S_{py}$ and a ~10‰ difference in $\Delta\delta^{34}$S are still apparent between the two sections, supporting our hypothesis for a lateral gradient in seawater sulfate concentration seemingly independent of correlation method. MFS: maximum flooding surface. $\Delta\delta^{13}$C is the difference between $\delta^{13}C_{carb}$ and $\delta^{13}C_{org}$.

**Table S1. Summary of chemostratigraphy data for the Ediacaran Doushanto Formation in South China (this study).**

| Sample | Depth | TOC | TIC | $S_{PY}$ | $TOC/S_{PY}$ | $\delta^{34}S_{Py}$ [1] | [CAS] | $\delta^{34}S_{CAS}$ [2] | $\Delta\delta^{34}S_{CAS-PY}$ [3] | Mo | Mo/TOC [4] | $Fe_{PY}$ | $Fe_{carb}$ | $Fe_{oxide}$ | $Fe_{mag}$ | $Fe_{HR}$ | $Fe_T$ | $Fe_{PY}/Fe_{HR}$ | $Fe_{HR}/Fe_T$ [5] | Al |
|---|---|---|---|---|---|---|---|---|---|---|---|---|---|---|---|---|---|---|---|---|
| | (m to Nantuo) | (wt %) | (wt %) | (wt %) | | (‰ VCDT) | (ppm in rock) | (‰ VCDT) | (‰ VCDT) | (ppm) | (ppm/wt%) | (wt %) | (wt %) | (wt %) | (wt %) | (wt %) | (wt %) | | | (wt %) |
| ***1. Inner shelf facies – Jiulongwan section*** | | | | | | | | | | | | | | | | | | | | |
| HN-23 | 154 | 15.1 | 1.1 | 2.2 | 6.8 | -13.5 | | | | 180.7 | 12.0 | 1.9 | 0.2 | 0.1 | 0.0 | 2.3 | 3.3 | 0.8 | 0.7 | 5.3 |
| HN-21 | 152 | 5.2 | 3.7 | 1.2 | 4.4 | -15.7 | 214.0 | 14.2 | 29.9 | 136.0 | 26.3 | 1.0 | 0.1 | 0.0 | 0.0 | 1.1 | 2.7 | 0.9 | 0.4 | 4.5 |
| HN-20 | 151 | | 1.0 | | | | 116.6 | 17.4 | | | | | | | | | | | | |
| HN-19 | 150 | | 1.4 | | | | 92.1 | 16.7 | | | | | | | | | | | | |
| HN-18 | 149 | 6.4 | 1.6 | 1.1 | 5.8 | -13.8 | 108.5 | 15.5 | 29.3 | 111.4 | 17.3 | 1.0 | 0.1 | 0.0 | 0.0 | 1.1 | 2.3 | 0.9 | 0.5 | 4.5 |
| HN-17 | 148 | | 1.3 | | | | 40.7 | 19.2 | | | | | | | | | | | | |
| HN-16 | 147 | | 0.5 | | | | 211.0 | 1.1 | | | | | | | | | | | | |
| HN-15 | 146 | 5.0 | 1.8 | 1.6 | 3.1 | -10.9 | 153.8 | 16.2 | 27.1 | 161.3 | 32.6 | 1.4 | 0.1 | 0.0 | 0.0 | 1.5 | 2.7 | 0.9 | 0.5 | 5.4 |
| HN-13 | 144 | 4.8 | 1.1 | 1.2 | 4.1 | -7.7 | | | | 71.8 | 15.1 | 1.0 | 0.1 | 0.0 | 0.0 | 1.1 | 2.9 | 0.9 | 0.4 | 5.5 |
| HN-09 | 144 | 4.6 | 0.9 | 2.2 | 2.1 | -7.4 | | | | 113.9 | 24.6 | 1.9 | 0.1 | 0.1 | 0.0 | 2.2 | 2.8 | 0.9 | 0.8 | 4.5 |
| HN-12 | 143 | 5.1 | 0.8 | 2.4 | 2.1 | -6.1 | | | | 125.1 | 24.5 | 2.1 | 0.1 | 0.1 | 0.0 | 2.3 | 3.1 | 0.9 | 0.8 | 4.4 |
| HN-11 | 142.2 | 2.0 | 0.6 | 2.4 | 0.8 | -10.7 | | | | 121.7 | 61.5 | 2.1 | 0.1 | 0.1 | 0.0 | 2.2 | 3.2 | 0.9 | 0.7 | 5.3 |
| HN-08 | 141.5 | 0.2 | 11.0 | 0.3 | 0.6 | -13.6 | 2991.9 | 34.3 | 47.9 | 0.6 | 3.3 | 0.3 | 0.1 | 0.0 | 0.0 | 0.4 | 0.5 | 0.7 | 0.7 | 0.9 |
| HN-10 | 140.9 | 0.3 | 10.8 | 0.4 | 0.6 | -7.6 | 11.2 | | | 2.8 | 10.2 | 0.4 | 0.1 | 0.0 | 0.0 | 0.5 | 0.7 | 0.7 | 0.8 | 0.9 |
| HN-06 | 140 | 0.2 | 10.6 | 0.3 | 0.6 | -8.0 | 104.6 | 29.7 | 37.7 | 1.6 | 7.5 | 0.3 | 0.2 | 0.0 | 0.1 | 0.6 | 0.8 | 0.5 | 0.7 | 1.2 |
| HN-07 | 138.5 | 0.1 | 10.8 | 0.3 | 0.3 | -6.9 | 32.5 | 26.9 | 33.8 | 1.2 | 16.1 | 0.2 | 0.2 | 0.0 | 0.1 | 0.6 | 0.8 | 0.4 | 0.7 | 1.1 |
| HN-05 | 113.3 | 0.2 | 10.3 | 0.3 | 0.7 | -2.9 | 149.2 | 20.8 | 23.7 | 1.0 | 4.2 | 0.3 | 0.1 | 0.0 | 0.0 | 0.5 | 0.6 | 0.6 | 0.8 | 0.8 |
| HN-04 | 105 | 0.0 | 9.6 | 0.6 | 0.0 | 2.4 | 102.1 | 28.6 | 26.2 | 1.1 | | 0.5 | 0.3 | 0.1 | 0.1 | 1.1 | 1.5 | 0.5 | 0.7 | 1.9 |
| HN-02 | 98 | 0.0 | 12.3 | 0.0 | 1.0 | -6.1 | 0.0 | | | 1.9 | | 0.0 | 0.1 | 0.2 | 0.0 | 0.3 | 0.4 | 0.0 | 0.9 | 0.3 |
| HN-01 | 92 | 0.0 | 11.8 | 0.0 | 1.0 | 11.5 | 0.0 | | | 1.2 | | 0.0 | 0.1 | 0.1 | 0.0 | 0.2 | 0.2 | 0.0 | 1.0 | 0.1 |
| JS-69 | 80 | | 6.0 | | | | 0.0 | | | | | | | | | | | | | |
| JS-68O | 79 | 0.7 | 6.4 | 0.8 | 0.9 | -0.3 | | | | 0.5 | 0.7 | 0.7 | 0.1 | 0.1 | 0.1 | 0.9 | 1.7 | 0.7 | 0.5 | 1.7 |
| JS-68I | 79 | 0.8 | 6.2 | 0.7 | 1.1 | 0.3 | 64.0 | 39.0 | 38.7 | 0.5 | 0.6 | 0.6 | 0.1 | 0.1 | 0.1 | 0.8 | 1.6 | 0.7 | 0.5 | 1.6 |
| JS-67 | 78 | | 5.9 | | | | 69.7 | 34.9 | | | | | | | | | | | | |
| JS-66 | 77 | | 4.2 | | | | 93.2 | 35.6 | | | | | | | | | | | | |
| JS-65 | 76 | | 7.1 | | | | 33.3 | 35.1 | | | | | | | | | | | | |
| JS-64 | 75 | 1.6 | 6.2 | 0.6 | 2.7 | 17.0 | 179.9 | 43.0 | 26.0 | 1.1 | 0.7 | 0.5 | 0.1 | 0.2 | 0.1 | 0.8 | 1.5 | 0.6 | 0.6 | 1.4 |
| JS-63 | 74 | | 5.0 | | | | 90.1 | 38.4 | | | | | | | | | | | | |
| JS-62 | 72.8 | | 6.9 | | | | 132.1 | 36.8 | | | | | | | | | | | | |
| JS-60 | 70 | 1.6 | 5.3 | 0.8 | 2.1 | 14.9 | 407.5 | 41.5 | 26.6 | 0.9 | 0.5 | 0.7 | 0.1 | 0.1 | 0.1 | 0.9 | 1.8 | 0.8 | 0.5 | 2.2 |
| JS-59 | 69 | | 7.6 | | | | 164.5 | 40.6 | | | | | | | | | | | | |
| JS-57 | 65 | | 5.7 | | | | 263.8 | 38.6 | | | | | | | | | | | | |
| JS-56 | 64 | 0.6 | 6.0 | 1.2 | 0.6 | 5.3 | 180.5 | 35.4 | 30.1 | 0.5 | 0.8 | 1.0 | 0.1 | 0.1 | 0.1 | 1.2 | 2.4 | 0.8 | 0.5 | 2.3 |
| JS-55 | 63 | | 5.5 | | | | 245.4 | 35.2 | | | | | | | | | | | | |
| JS-54 | 62 | | 5.8 | | | | 246.5 | 47.7 | | | | | | | | | | | | |
| JS-52 | 60 | | 6.5 | | | | 483.1 | 48.2 | | | | | | | | | | | | |
| JS-51 | 59 | 0.6 | 7.6 | 0.6 | 1.0 | 7.4 | 0.0 | | | 0.4 | 0.6 | 0.5 | 0.2 | 0.1 | 0.0 | 0.8 | 1.4 | 0.6 | 0.6 | 1.0 |
| JS-48 | 56 | 1.0 | 7.1 | 0.6 | 1.7 | 3.4 | 113.8 | 33.8 | 30.4 | 0.3 | 0.3 | 0.5 | 0.1 | 0.1 | 0.1 | 0.8 | 1.7 | 0.7 | 0.4 | 1.4 |
| JS-47 | 55 | | 5.6 | | | | 277.9 | 40.3 | | | | | | | | | | | | |
| JS-45 | 52 | 0.7 | 7.9 | 0.5 | 1.5 | 9.5 | 73.2 | 38.0 | 28.5 | 0.4 | 0.5 | 0.4 | 0.1 | 0.1 | 0.1 | 0.7 | 1.1 | 0.6 | 0.6 | 0.9 |
| JS-44 | 51 | | 7.7 | | | | 88.6 | 48.3 | | | | | | | | | | | | |
| JS-42 | 49 | 0.9 | 6.4 | 0.9 | 0.9 | 4.7 | 190.4 | 32.6 | 27.9 | 0.8 | 0.9 | 0.8 | 0.1 | 0.1 | 0.1 | 1.2 | 2.3 | 0.7 | 0.5 | 2.0 |
| JS-40 | 41 | 1.1 | 5.9 | 0.1 | 22.4 | -12.6 | 220.3 | 36.2 | 48.8 | 0.4 | 0.4 | 0.0 | 0.0 | 1.2 | 0.1 | 1.4 | 2.5 | 0.0 | 0.6 | 2.7 |
| JS-39 | 40 | | 6.7 | | | | 52.3 | 31.5 | | | | | | | | | | | | |
| JS-37 | 38 | 0.8 | 5.8 | 0.0 | 19.0 | 20.1 | 93.6 | 44.0 | 23.9 | 0.4 | 0.5 | 0.0 | 0.1 | 0.8 | 0.0 | 1.0 | 1.6 | 0.0 | 0.6 | 1.2 |
| JS-35 | 35.6 | | 8.0 | | | | 76.0 | 41.2 | 24.6 | | | | | | | | | | | |
| JS-34 | 35 | 0.9 | 5.8 | 0.0 | 29.3 | 16.6 | 0.0 | | | 0.1 | 0.1 | 0.0 | 0.1 | 0.1 | 0.0 | 0.2 | 0.2 | 0.1 | 0.9 | 0.2 |
| JS-32 | 33 | | 5.7 | | | | 79.7 | 35.5 | | | | | | | | | | | | |
| JS-31 | 32 | | 5.9 | | | | 121.8 | 34.3 | | | | | | | | | | | | |
| JS-29 | 30 | 1.2 | 5.8 | 0.0 | 31.0 | 8.7 | 24.4 | 33.2 | 24.5 | 0.3 | 0.3 | 0.0 | 0.1 | 0.9 | 0.1 | 1.1 | 1.9 | 0.0 | 0.6 | 1.7 |
| JS-28 | 29 | | 5.9 | | | | 78.3 | 30.5 | 21.8 | | | | | | | | | | | |
| JS-26 | 25 | 0.7 | 7.4 | 0.3 | 2.8 | 3.2 | 0.0 | | | 0.2 | 0.3 | 0.2 | 0.1 | 0.2 | 0.0 | 0.6 | 1.2 | 0.4 | 0.5 | 0.9 |
| JS-24 | 19.7 | 2.9 | 4.2 | 1.3 | 2.3 | 23.6 | 544.0 | 34.0 | 10.4 | 1.6 | 0.6 | 1.1 | 0.1 | 0.1 | 0.1 | 1.3 | 2.5 | 0.8 | 0.5 | 2.6 |
| JS-22 | 17.5 | | 7.5 | | | | 128.9 | 34.6 | 22.9 | | | | | | | | | | | |
| JS-21 | 16 | 1.8 | 5.5 | 1.1 | 1.7 | 11.7 | 246.9 | 33.7 | 22.0 | 1.1 | 0.6 | 0.9 | 0.1 | 0.0 | 0.0 | 1.1 | 1.9 | 0.8 | 0.6 | 1.9 |
| JS-18 | 8 | 1.2 | 6.5 | 1.4 | 0.9 | 18.7 | 261.7 | 34.7 | 16.0 | 1.3 | 1.1 | 1.2 | 0.1 | 0.2 | 0.1 | 1.5 | 2.4 | 0.8 | 0.6 | 2.1 |
| JS-17 | 6 | 0.5 | 7.1 | 1.8 | 0.3 | 17.4 | 187.5 | 34.1 | 16.7 | 1.7 | 3.3 | 1.5 | 0.1 | 0.1 | 0.0 | 1.8 | 2.3 | 0.8 | 0.8 | 1.7 |
| JS-15* | 5.3 | 0.1 | 7.4 | 0.9 | 0.1 | 19.5 | 142.3 | 41.2 | 21.7 | 0.0 | 0.0 | 0.7 | 0.1 | 0.0 | 0.0 | 0.9 | 1.9 | 0.8 | 0.5 | 2.3 |
| JS-16* | 4 | 0.0 | 9.7 | 0.3 | 0.1 | 27.9 | 59.6 | 45.1 | 17.2 | 0.9 | | 0.3 | 0.1 | 0.0 | 0.0 | 0.4 | 0.5 | 0.6 | 0.9 | 0.4 |
| HJ-02* | 1.6 | 0.2 | 11.6 | 0.1 | 2.2 | 36.1 | 62.3 | 41.1 | 5.0 | 0.8 | 5.3 | 0.1 | 0.1 | 0.0 | 0.0 | 0.2 | 0.3 | 0.3 | 0.7 | 0.4 |
| HJ-03* | 1.3 | 0.0 | 12.0 | 0.1 | 0.2 | 42.2 | 37.7 | 29.0 | -13.2 | 0.8 | | 0.1 | 0.1 | 0.0 | 0.0 | 0.2 | 0.3 | 0.3 | 0.6 | 0.5 |
| JS-12* | 1.25 | 0.0 | 10.1 | 0.1 | 0.1 | 18.7 | | 28.4 | 9.7 | 0.9 | | 0.1 | 0.1 | 0.0 | 0.0 | 0.2 | 0.3 | 0.5 | 0.7 | 0.6 |
| JS-13* | 0.75 | 0.2 | 11.8 | 0.0 | 17.0 | 29.0 | | 30.5 | 1.5 | 0.0 | 0.1 | 0.0 | 0.2 | 0.1 | 0.0 | 0.3 | 0.4 | 0.0 | 0.8 | 0.4 |
| HJ-01* | 0.7 | 0.0 | 11.7 | 0.1 | 0.3 | 33.2 | | 41.2 | 8.0 | 0.9 | | 0.1 | 0.1 | 0.0 | 0.0 | 0.2 | 0.2 | 0.2 | 0.9 | 0.3 |
| JS-14* | 0.1 | 0.5 | 9.5 | 3.9 | 0.1 | 41.4 | | 40.1 | -1.3 | 3.9 | 7.8 | 3.4 | 0.2 | 0.5 | 0.0 | 4.2 | 4.1 | 0.8 | 1.0 | 0.5 |
| ***2. Shelf margin facies – Zhongling section*** | | | | | | | | | | | | | | | | | | | | |
| SH-41 | 287 | | 7.4 | | | | 327.8 | 44.5 | 22.5 | | | | | | | | | | | |
| SH-42 | 286 | 0.1 | 3.6 | 0.9 | 0.1 | 22.0 | 0.0 | | | 0.4 | 4.2 | 0.8 | 0.0 | 0.0 | 0.0 | 0.8 | 0.9 | 1.0 | 0.8 | 0.7 |
| SH-79 | 284.5 | 0.6 | 6.8 | 0.2 | 4.2 | 16.8 | 473.7 | 36.9 | 20.1 | 0.1 | 0.1 | 0.1 | 0.0 | 0.0 | 0.0 | 0.2 | 0.2 | 0.8 | 1.0 | 0.1 |
| SH-44 | 282 | 0.0 | 9.5 | 0.1 | 0.1 | 22.3 | 0.0 | | | 0.1 | | 0.1 | 0.0 | 0.0 | 0.0 | 0.1 | 0.1 | 0.7 | 1.0 | 0.1 |
| SH-46 | 278 | | 4.9 | | | | 0.0 | | | | | | | | | | | | | |
| SH-47 | 275 | 0.4 | 6.5 | 0.1 | 5.0 | 17.5 | 0.0 | | | 0.3 | 0.9 | 0.1 | 0.0 | 1.0 | 0.0 | 1.1 | 1.4 | 0.1 | 0.8 | 1.4 |
| SH-45 | 274 | | 4.0 | | | | 1814.3 | 38.7 | 21.2 | | | | | | | | | | | |
| SH-48 | 272 | 1.0 | 5.2 | 0.1 | 8.1 | 9.5 | 0.0 | | | 0.7 | 0.7 | 0.1 | 0.0 | 1.8 | 0.0 | 1.9 | 2.5 | 0.1 | 0.8 | 2.1 |
| SH-50 | 269 | 0.0 | 11.8 | 0.0 | 0.2 | 18.7 | 19.7 | 39.3 | 20.6 | 0.1 | | 0.0 | 0.0 | 0.0 | 0.0 | 0.1 | 0.1 | 0.5 | 1.0 | 0.0 |
| SH-80 | 266 | 0.2 | 11.4 | 0.0 | 5.4 | 16.2 | 63.6 | 30.5 | 14.3 | 0.1 | 0.2 | 0.0 | 0.0 | 0.0 | 0.0 | 0.1 | 0.0 | 0.5 | 1.6 | 0.0 |
| SH-62 | 223 | 0.3 | 9.7 | 0.1 | 4.0 | 22.8 | 4.4 | 39.9 | 17.1 | 0.2 | 0.8 | 0.1 | 0.1 | 0.3 | 0.0 | 0.5 | 0.6 | 0.1 | 0.9 | 0.4 |
| SH-61 | 221 | 0.5 | 10.4 | 0.1 | 7.0 | 23.0 | 26.6 | 40.3 | 17.3 | 0.4 | 0.7 | 0.1 | 0.1 | 0.2 | 0.0 | 0.3 | 0.3 | 0.2 | 1.0 | 0.3 |
| SH-60 | 219 | | 10.4 | | | | 0.0 | | | | | | | | | | | | | |
| SH-59 | 217 | 0.4 | 9.6 | 0.1 | 4.3 | 23.3 | 0.0 | | | 0.2 | 0.5 | 0.1 | 0.1 | 0.2 | 0.0 | 0.3 | 0.3 | 0.3 | 0.9 | 0.3 |
| SH-57 | 213 | 0.3 | 9.7 | 0.0 | 9.8 | 24.2 | 10.9 | 44.7 | 20.5 | 0.2 | 0.5 | 0.0 | 0.1 | 0.3 | 0.0 | 0.3 | 0.4 | 0.1 | 0.9 | 0.3 |
| SH-56 | 210.5 | 0.6 | 9.1 | 0.0 | 21.6 | 23.5 | 0.0 | | | 0.2 | 0.4 | 0.0 | 0.0 | 0.3 | 0.0 | 0.4 | 0.4 | 0.1 | 0.9 | 0.3 |
| SH-55 | 208 | 0.7 | 8.7 | 0.1 | 11.2 | 23.6 | 32.6 | 44.6 | 21.0 | 0.3 | 0.5 | 0.1 | 0.0 | 0.4 | 0.0 | 0.5 | 0.5 | 0.1 | 0.9 | 0.4 |

| Sample | Depth | TOC | TIC | $S_{PY}$ | $TOC/S_{PY}$ | $\delta^{34}S_{Py}$ [1] | [CAS] | $\delta^{34}S_{CAS}$ [2] | $\Delta\delta^{34}S_{CAS-PY}$ [3] | Mo | Mo/TOC [4] | $Fe_{PY}$ | $Fe_{carb}$ | $Fe_{oxide}$ | $Fe_{mag}$ | $Fe_{HR}$ | $Fe_T$ | $Fe_{PY}/Fe_{HR}$ | $Fe_{HR}/Fe_T$ [5] | Al |
|---|---|---|---|---|---|---|---|---|---|---|---|---|---|---|---|---|---|---|---|---|
| | (m to Nantuo) | (wt %) | (wt %) | (wt %) | | (‰ VCDT) | (ppm in rock) | (‰ VCDT) | (‰ VCDT) | (ppm) | (ppm/wt%) | (wt %) | (wt %) | (wt %) | (wt %) | (wt %) | (wt %) | | | (wt %) |
| SH-54 | 206 | | 9.6 | | | | 0.0 | | | | | | | | | | | | | |
| SH-53 | 204 | 0.6 | 10.4 | 0.1 | 12.9 | 26.0 | 0.0 | | | 0.1 | 0.2 | 0.0 | 0.0 | 0.1 | 0.0 | 0.2 | 0.2 | 0.2 | 1.0 | 0.2 |
| SH-52 | 202 | | 9.8 | | | | 0.1 | | | | | | | | | | | | | |
| SH-51 | 200 | 0.3 | 10.1 | 0.1 | 6.4 | 22.7 | 0.0 | | | 0.1 | 0.4 | 0.0 | 0.1 | 0.2 | 0.1 | 0.4 | 0.4 | 0.1 | 1.0 | 0.3 |
| SH-71 | 154.5 | 0.6 | 7.8 | 0.0 | 41.9 | 27.4 | 0.6 | 49.5 | 22.1 | 0.3 | 0.5 | 0.0 | 0.1 | 0.7 | 0.1 | 0.9 | 1.1 | 0.0 | 0.8 | 0.9 |
| SH-70 | 152 | | 8.9 | | | | 0.0 | | | | | | | | | | | | | |
| SH-69 | 151 | 1.0 | 7.4 | 0.0 | 21.7 | 26.2 | 0.0 | | | 0.5 | 0.6 | 0.0 | 0.2 | 0.6 | 0.1 | 0.9 | 1.2 | 0.0 | 0.8 | 0.9 |
| SH-67 | 146 | 0.7 | 8.7 | 0.1 | 13.0 | 26.0 | 10.5 | 45.7 | 19.7 | 0.3 | 0.4 | 0.0 | 0.1 | 0.2 | 0.0 | 0.4 | 0.4 | 0.1 | 0.9 | 0.3 |
| SH-65 | 142 | 0.0 | 9.4 | 0.1 | 0.2 | 22.0 | 0.0 | | | 0.2 | | 0.1 | 0.1 | 0.2 | 0.0 | 0.4 | 0.5 | 0.2 | 0.8 | 0.3 |
| SH-63 | 138 | 0.2 | 8.7 | 0.0 | 5.0 | 24.4 | 0.0 | | | 0.1 | 0.6 | 0.0 | 0.2 | 0.4 | 0.0 | 0.7 | 0.9 | 0.0 | 0.7 | 0.5 |
| SH-72 | 126 | 0.1 | 11.0 | 0.1 | 1.4 | 35.9 | 79.4 | 60.1 | 24.2 | 0.2 | 1.8 | 0.1 | 0.0 | 0.1 | 0.0 | 0.2 | 0.1 | 0.4 | 1.0 | 0.1 |
| SH-73 | 124 | 0.1 | 10.8 | 0.1 | 0.8 | 26.7 | 189.4 | 47.6 | 20.9 | 0.3 | 2.9 | 0.1 | 0.0 | 0.0 | 0.0 | 0.2 | 0.1 | 0.7 | 1.0 | 0.1 |
| SH-74 | 123 | | 10.2 | | | | 161.3 | 41.5 | 14.8 | | | | | | | | | | | |
| SH-75 | 114 | | 8.1 | | | | 20.3 | 38.1 | 8.7 | | | | | | | | | | | |
| SH-76 | 112 | 1.8 | 7.6 | 0.1 | 34.9 | 29.4 | 0.0 | | | 0.8 | 0.5 | 0.0 | 0.1 | 0.5 | 0.0 | 0.6 | 0.9 | 0.1 | 0.7 | 0.9 |
| SH-77 | 110 | | 10.1 | | | | 0.0 | | | | | | | | | | | | | |
| SH-78 | 108 | 1.2 | 8.5 | 0.1 | 15.1 | 33.2 | 0.0 | | | 0.6 | 0.5 | 0.1 | 0.0 | 0.3 | 0.0 | 0.4 | 0.5 | 0.2 | 0.9 | 0.5 |
| SH-40 | 81 | 0.3 | 11.6 | 0.1 | 4.8 | 23.5 | 0.0 | | | 0.1 | 0.4 | 0.1 | 0.1 | 0.0 | 0.0 | 0.2 | 0.2 | 0.3 | 1.0 | 0.1 |
| SH-35 | 77.6 | 0.2 | 1.5 | 0.0 | 4.4 | 30.1 | 0.0 | | | 0.2 | 0.9 | 0.0 | 0.3 | 0.5 | 0.0 | 0.8 | 5.2 | 0.0 | 0.2 | 4.5 |
| SH-37 | 75 | 0.1 | 0.1 | 0.0 | 3.1 | 23.4 | | | | 0.1 | 1.3 | 0.0 | 0.2 | 0.1 | 0.2 | 0.5 | 7.7 | 0.1 | 0.1 | 4.5 |
| SH-38 | 73.5 | 0.1 | 1.6 | 0.0 | 2.9 | 21.1 | 0.0 | | | 0.1 | 1.2 | 0.0 | 0.4 | 0.3 | 0.0 | 0.7 | 6.7 | 0.0 | 0.1 | 4.1 |
| SH-34 | 37 | 0.8 | 0.5 | 0.1 | 7.7 | 7.2 | | | | 0.2 | 0.2 | 0.1 | 0.9 | 0.5 | 0.9 | 2.4 | 4.3 | 0.0 | 0.6 | 6.2 |
| SH-31 | 33.5 | 0.2 | 0.0 | 0.0 | | n.d. | | | | 0.0 | 0.1 | 0.0 | 0.0 | 0.9 | 0.1 | 1.0 | 5.1 | 0.0 | 0.2 | 6.5 |
| SH-28 | 31 | 3.4 | 0.0 | 0.1 | 59.3 | -10.6 | | | | 8.9 | 2.6 | 0.0 | 0.1 | 0.3 | 0.0 | 0.4 | 1.1 | 0.1 | 0.4 | 5.5 |
| SH-26 | 29 | 0.7 | 0.4 | 1.5 | 0.4 | -9.0 | | | | 4.7 | 7.1 | 1.3 | 0.2 | 0.2 | 0.1 | 1.9 | 2.8 | 0.7 | 0.7 | 5.1 |
| SH-24 | 27 | 3.8 | 0.3 | 2.9 | 1.3 | -11.2 | | | | 9.6 | 2.5 | 2.5 | 0.1 | 0.5 | 0.2 | 3.4 | 4.1 | 0.7 | 0.8 | 5.4 |
| SH-23 | 19.5 | 2.9 | 0.0 | 2.3 | 1.3 | -11.2 | | | | 12.7 | 4.3 | 2.0 | 0.4 | 0.2 | 0.0 | 2.7 | 3.7 | 0.8 | 0.7 | 5.7 |
| SH-20 | 17 | 3.0 | 0.0 | 2.2 | 1.3 | -17.2 | | | | 6.0 | 2.0 | 1.9 | 0.3 | 0.8 | 0.0 | 3.1 | 4.1 | 0.6 | 0.7 | 5.1 |
| SH-18 | 14.5 | 2.0 | 0.0 | 3.3 | 0.6 | -17.2 | | | | 12.4 | 6.1 | 2.9 | 0.2 | 0.2 | 0.0 | 3.3 | 3.9 | 0.9 | 0.8 | 5.1 |
| SH-16 | 12.8 | 1.0 | 0.0 | 0.0 | 103.2 | 1.7 | | | | 4.2 | 4.0 | 0.0 | 0.0 | 0.5 | 0.0 | 0.6 | 1.7 | 0.0 | 0.3 | 6.4 |
| SH-15 | 9.1 | 0.5 | 0.0 | 0.2 | 2.6 | -15.1 | | | | 4.4 | 9.4 | 0.2 | 0.0 | 1.3 | 0.0 | 1.6 | 2.4 | 0.1 | 0.7 | 6.6 |
| SH-13 | 7.5 | 0.1 | 5.3 | 2.0 | 0.1 | 9.1 | 0.0 | | | 0.7 | 5.2 | 1.7 | 0.4 | 0.1 | 0.1 | 2.3 | 2.6 | 0.7 | 0.9 | 3.6 |
| SH-10* | 6 | | 12.0 | | | | 0.0 | | | | | | | | | | | | | |
| SH-12* | 4 | | 11.4 | | | | 0.0 | | | | | | | | | | | | | |
| SH-14* | 0.1 | | 12.3 | | | | 0.0 | | | | | | | | | | | | | |
| ***3. Slope facies – Minle section*** | | | | | | | | | | | | | | | | | | | | |
| ML-21 | 8 | 1.0 | 0.0 | 0.0 | 103.0 | n.d. | 0.0 | | | 3.9 | 3.8 | 0.0 | 0.0 | 0.4 | 0.1 | 0.5 | 2.5 | 0.0 | 0.2 | 7.3 |
| ML-20 | 7 | 0.3 | 4.4 | 0.1 | 4.0 | -20.7 | 0.0 | | | 0.1 | 0.3 | 0.1 | 0.3 | 0.9 | 0.1 | 1.4 | 4.2 | 0.0 | 0.3 | 4.6 |
| ML-19 | 6 | 0.2 | 3.2 | 0.0 | 7.0 | -18.7 | 0.0 | | | 0.1 | 0.6 | 0.0 | 0.4 | 0.1 | 0.1 | 0.7 | 3.0 | 0.0 | 0.2 | 5.4 |
| ML-23* | 4 | 0.0 | 12.2 | 0.0 | 1.0 | n.d. | | 24.6 | | 0.1 | | 0.0 | 0.3 | 0.1 | 0.0 | 0.4 | 0.6 | 0.0 | 0.7 | 0.5 |
| ***4. Basinal facies – Longe section*** | | | | | | | | | | | | | | | | | | | | |
| ZH07-30 | 14.5 | 1.8 | 0.0 | 0.0 | 184.0 | n.d | | | | 0.5 | 0.3 | 0.0 | 0.0 | 0.0 | 0.0 | 0.1 | 0.2 | 0.2 | 0.4 | 2.4 |
| ZH07-28 | 9 | 3.5 | 0.0 | 0.0 | 352.0 | n.d | | | | 3.1 | 0.9 | 0.0 | 0.0 | 0.1 | 0.0 | 0.1 | 0.3 | 0.1 | 0.2 | 5.2 |
| ZH07-26 | 7 | 2.1 | 0.0 | 0.0 | 209.0 | n.d | | | | 4.5 | 2.1 | 0.0 | 0.0 | 0.1 | 0.0 | 0.1 | 0.4 | 0.1 | 0.2 | 6.4 |
| ZH07-23 | 5 | 3.6 | 0.0 | 0.0 | 359.0 | n.d | | | | 10.1 | 2.8 | 0.0 | 0.0 | 0.0 | 0.0 | 0.0 | 0.3 | | 0.0 | 5.9 |
| ZH07-25* | 4 | 0.3 | 12.1 | 0.4 | 0.6 | 0.4 | 0.0 | | | 1.1 | 4.4 | 0.3 | 0.2 | 0.1 | 0.1 | 0.6 | 0.8 | 0.5 | 0.8 | 0.3 |
| ZH07-22* | 3 | 0.0 | 12.2 | 0.0 | 1.0 | n.d | 0.0 | | | 0.7 | | 0.0 | 0.1 | 0.1 | 0.0 | 0.2 | 0.3 | 0.0 | 0.7 | 0.2 |

1. "n.d.": insufficient pyrite content.
2. Samples with carbonate contents <30% were not extracted for CAS.
3. For samples with $\delta^{34}S_{CAS}$ values but no $\delta^{34}S_{py}$ data from the same sample; best estimates for $\delta^{34}S_{py}$ are based on adjacent samples.
4. For samples with TOC < 0.05%, we did not calculate Mo/TOC ratios due to large uncertainties in the TOC contents.
5. For samples with calculated $Fe_{HR}/Fe_T > 1$, the ratio is considered to be 1.
6. *cap carbonate samples.

**References:**


S1. D. E. Canfield, R. Raiswell, J. T. Westrich, C. M. Reaves. R. A. Berner. *Chem. Geol.* **54**, 149-155 (1986).
S2. S. W. Poulton, D. E. Canfield, *Chem. Geol.* **214**, 209-221 (2005).
S3. K. A. McFadden *et al. Proc. Natl Acad. Sci.USA* **105**, 3197-3202 (2008).
S4. G. Jiang, A. J. Kaufman, N. Christie-Blick, S. Zhang, H. Wu, *Earth Planet. Sci. Lett.* **261**, 303-320 (2007).
S5. G. Jiang, M. J. Kennedy, N. Christie-Blick, *Nature* **426**, 822-826 (2003).
S6. M. Y. Zhu, J. M. Zhang, A. H. Yang, *Palaeogeogr. Palaeoclimatol. Palaeoecol.* **254**, 7-61(2007).
S7. D. Condon, M. Zhu, S. Bowring, W. Wang, J. Yang, *Science* **308**, 95-98 (2005).
S8. P. Liu, C. Yin, L. Gao, F. Tang, S. Chen, *Chinese Sci Bull* **54**, 1058-1064 (2009).
S9. Y. Shen, D. E. Canfield, A. H. Knoll, *Am. J. Sci.* **302**, 81-109 (2002).
S10. Y. Shen, A. H. Knoll, M. R. Walter, *Nature* **423**, 632-635 (2003).
S11. S. W. Poulton, P. W. Fralick, D. E. Canfield, *Nature* **431**, 173-177 (2004).
S12. R. Raiswell et al., *Am. J. Sci.* **308**, 105-129 (2008).
S13. C. Scott et al. *Nature* **452**, 456-459 (2008).
S14. D. A. Fike, J. P. Grotzinger, L. M. Pratt, R. E. Summons, *Nature* **444**, 744-747 (2006).
S15. T. F. Bristow et al., *Proc. Natl Acad. Sci.USA* **106**, 13190-13195 (2009).
S16. R. A. Berner, *Geochim. Cosmochim. Acta* **48**, 605-615 (1984).
S17. R. A. Berner, R. Raiswell, *Geochim. Cosmochim. Acta* **47**, 855-862 (1983).
S18. R. A. Berner, R. Raiswell, *Geology* **12**, 365-368 (1984).
S19. P. A. Cohen, A. H. Knoll, R. B. Kodner, *Proc. Natl Acad. Sci. USA* **106**, 6519-6524 (2009).